Using UWB Measurements for Statistical Analysis of the Ranging Error in Indoor Multipath Environment

BARDIA ALAVI, KAVEH PAHLAVAN, NAYEF ALSINDI

CWINS, ECE Dept., Worcester Polytechnic Institute,

100 Institute Rd., Worcester, MA 01609, USA

{bardia, kaveh, nalsindi}@wpi.edu

XINRONG LI

Department of Electrical Engineering, College of Engineering

University of North TexasUniversity

3940 N. Elm St., Denton, TX 76207, USA

xinrong@unt.edu

Abstract: In this paper we use UWB measurements for bandwidths up to 3GHz to present a framework for statistical modeling of the indoor radio channel propagation characteristics that are pertinent to precise indoor geolocation using time-of-arrival (TOA) estimations. Accuracy of indoor geolocation systems relies on the strength and TOA of the direct path (DP) in the channel profile. Based on UWB measurements in a typical office building, we introduce empirical models for the path-loss and TOA of the DP. We use path-loss model for the DP to analyze the occurrence of the undetected direct path (UDP) conditions which cause large errors in indoor geolocation systems. Then we introduce a novel statistical model for the ranging or distance measurement error (DME) which is needed for comparative performance evaluation of the indoor positioning algorithms. The DME is a function of the bandwidth of the system, occurrence of the UDP conditions, and the distance between the transmitter and the receiver.

Keywords: Radio propagation, positioning, ultra wideband, time of arrival, ranging

1   Introduction

Ultra-wideband (UWB) technology has been one of the major developments in recent years in wireless industry [Opp04] [Ghav04]. Currently, most of the UWB channel measurement and modeling results are focused on short-range (<10m) high-rate applications [Mol03] while the UWB technology has the potential to trade a reduced data rate for increased range, and potentially, accurate positioning capabilities [Por03]. Accurate positioning systems are extremely useful in many commercial, public safety and military applications, such as tracking and navigation for firefighters or soldiers in hostile environments [Pah02].

Channel modeling for telecommunication and precise positioning in multipath rich indoor environments involve different emphasis on measurement requirements and modeling [Pah98, Pah02, and Li04]. In telecommunication applications we are interested in measurement and modeling of the behavior of the multipath spread of the channel [Sal87, Has93, Rap02, Ghas03, Cas02, and Mol03]. In indoor geolocation applications we place greater emphasis on the behavior of the direct path between the transmitter and the receiver antennas which becomes very complex in non-line-of-sight (NLOS) conditions causing large positioning errors. Currently there

is no model in the literature to address the statistical behavior of the direct path and the resulting ranging errors. These models are needed for development of future indoor geolocation algorithms which are expected to mitigate the effects of large ranging errors due to behavior of the direct path in the channel. This paper provides a framework for development of these models.

Multipath channel impulse response is usually modeled as [Sal87, Rap02, Pah05],

$$h(\tau) = \sum_{k=1}^{L_p} \alpha_k \delta(\tau - \tau_k) , \qquad (1)$$

where L_p is the number of multipath components, and $\alpha_k = |\alpha_k| e^{j\phi_k}$ and τ_k are amplitude and propagation delay of the kth path, respectively. To make discussions simpler, we define the direct line-of-sight (LOS) path between transmitter and receiver antennas as the *direct-path* (DP) and the detected first arrival path in the measured channel impulse response as the *first-detected-peak* (FDP). In time-of-arrival (TOA) based positioning systems, the TOA of the FDP $\hat{\tau}$ is detected as an estimate of the TOA of the DP, τ_{DP}, the estimated distance between the transmitter and the receiver antennas are obtained from $\hat{d} = c \times \hat{\tau}$, where c is the speed of light. The ranging error or distance measurement error (DME) is then defined as $DME = \hat{d} - d$, where d is the spatial distance between transmitter and receiver antennas. In practice, the empirical analysis of the DME is a function of the accuracy of measurement of the DP which is a function of the bandwidth of the measurement system. UWB measurements provide the widest bandwidth and consequently the most accurate measurements of the behavior of the DP. In this paper we use UWB measurements in a typical office building to introduce a framework for developing empirical models for the behavior of the DP. We emphasize the NLOS environments for which the undetected direct path (UDP) conditions cause unexpectedly large DME, posing a serious challenge to development of algorithms for precise indoor geolocation. We first develop an empirical path-loss model for the DP and we explain how this model can be used to explain the occurrence of UDP conditions. Then, based on the results of path-loss modeling we introduce a novel model for the behavior of the DME as a function of bandwidth of the system, occurrence of the UDP conditions, and the distance between the transmitter and the receiver antennas.

The organization of the rest of this paper is as follows. In section 2 we introduce the principles behind modeling of ranging error in multipath rich indoor environments. These principles are used for empirical models introduced in sections 4 and 5. Section 3; describe the UWB measurement system and the collected database for the empirical modeling. In section 4 we use this database to develop empirical path-loss models for the total power and the power of the DP. We use these path-loss models to identify regions with different behavior for the DME. In sections 5 we analyze the causes of DME and based on that in section 6 we provide the details of a novel model for behavior of the DME in different regions.

2   Ranging Error in Multipath Rich Indoor Areas

Ranging error or DME is a function of bandwidth of the system and occurrence of the UDP conditions which are both results of multipath structure of the channel between the transmitter and the receiver antennas. In this section through examples and analysis we provide a background for intuitive understanding of the relationship among bandwidth of the system, DME, and path-loss models for the power of the DP in multipath rich indoor areas.

2.1 Bandwidth, multipath, and DME

Figure 1-a shows the basic concepts involved in the wideband TOA measurement using arrival time of the DP in a typical indoor multipath environment [Ala03a]. In this figure the solid vertical lines represent the ideal channel impulse response generated by a ray-tracing algorithm for two arbitrary locations in an office area. In this channel profile the DP is also the strongest path and location of this path is the expected value of the TOA. Other paths arriving after a number of reflections and transmissions occur after the DP with lower amplitudes. These paths generated by ray-tracing algorithms would have been observed at the receiver if the bandwidth of the system was infinite. In practice bandwidth is limited and the received signal will be a number of pulses whose amplitude and arrival time are the same as impulses but they have a pulse shape and addition of all these pulse shapes forms the received signal, which in Fig. 1-a we refer to as the channel profile [pah05]. In indoor geolocation systems we use the first detected peak of the channel profile above the detection threshold as the estimated TOA of the DP. In a single path environment the actual expected and the estimated DP are the same. In multipath conditions, however, as shown in Fig. 1-a, the peak of the channel profile gets shifted from the expected TOA resulting in a TOA estimation error caused by the multipath condition. We refer to the ranging error caused by erroneous estimate of the TOA as DME. For a given multipath condition we expect that as we increase the bandwidth DME reduces [Ala03b].

2.2 Example occurrence of UDP conditions

As we explained earlier in NLOS multipath conditions when the DP goes below the detection threshold while other paths are detectable, the receiver assumes the FDP in the profile to be the DP and this mistake causes large DMEs. We refer to this situation the UDP condition [Pah98]. Figure 1-b shows an example of the occurrence of a large error due to a UDP condition, obtained from the results of ray-tracing for a transmitted pulse with a bandwidth of 200MHz. Since the difference between the strength of the strongest path and the DP is more than the dynamic range (the range of detectable signal level below the strongest path) of the receiver, we have a clear UDP condition in which the FDP estimated as the DP resulting in a 5.23m DME.
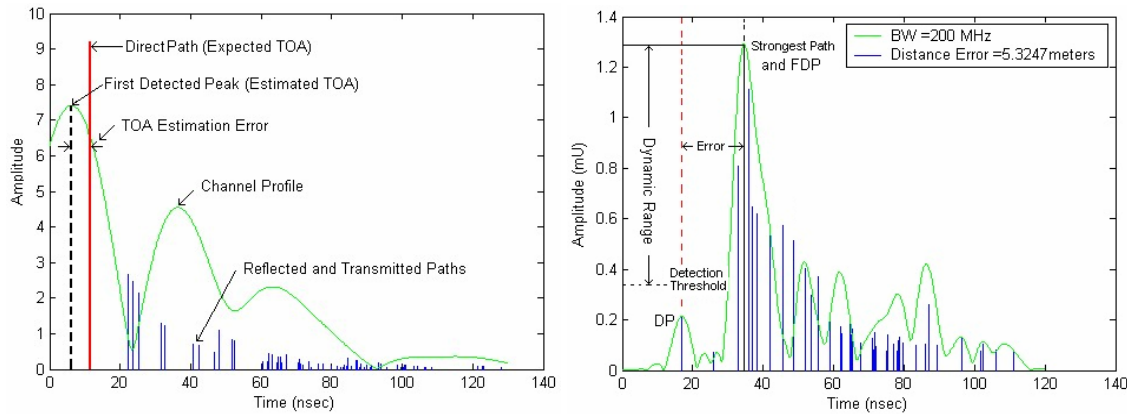
Figure 1: (a) Parameters involved in wideband TOA measurement using the arrival of DP, (b) UDP multipath condition from results of ray-tracing simulation and a channel profile with 200 MHz.

2.3 Path-loss modeling and UDP conditions

In this sub-section, using path-loss models for total power and the DP, we show that the frequent occurrence of the UDP conditions in multipath rich environments is unavoidable. As a mobile terminal moves away from a base station both the strength of the DP and the total received signal power decay exponentially. Figure 2 illustrates the decaying behavior of these two signals. At first-meter distance path-loss for the total power and the DP are the same, as the distance

3

increases the DP power attenuates much faster than the total power. With this observation, the distances from the transmitter can be divided into three regions: DDP (Detected DP), UDP, and NC (No-Coverage) regions. In DDP region accurate ranging is achievable since the DP is detectable; in UDP region system has coverage for data communication but the ranging error for geolocation applications can be very large; in NC region, system has no coverage at all. This discussion suggests that UDP conditions always exist and if we have a path-loss model for the DP we can identify this area from which we can find the statistics of occurrence of UDP conditions [Ala05].
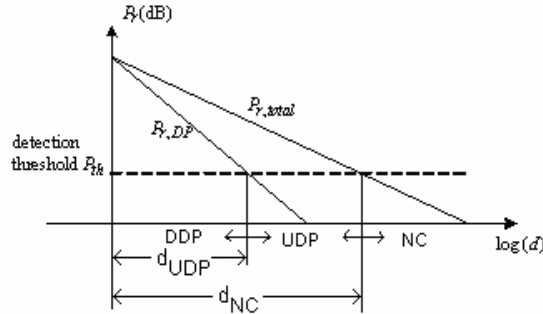
Figure 2: Illustration of DDP, UDP and NC regions in positioning applications.

3 UWB Measurements for Ranging Errors

UWB measurements provide the best resolution for detection of the DP and as such they are the most useful for radio propagation modeling applied to indoor geolocation. To develop empirical models for the behavior of the DP we need a database of measurements in a typical application scenario. This database of channel profiles accompanied by measured physical distances between the transmitter and the receiver antennas for each measurement and needs further post processing to extract parameter pertinent to indoor geolocation application.

3.1 Measurement system

The system used is a frequency-domain measurement system, originally introduced in [How90]. It employs a 40GHz Agilent E8363B vector network analyzer that is used to sweep the frequency spectrum from 3-6 GHz with frequency sampling interval of 1 MHz. Figure 3 shows the measurement system. The transmitter and the receiver are a pair of disc-cone UWB antennas which are connected to the network analyzer by low-loss cables. On the receiver side a low-noise amplifier (LNA) is connected between the antenna and the network analyzer.
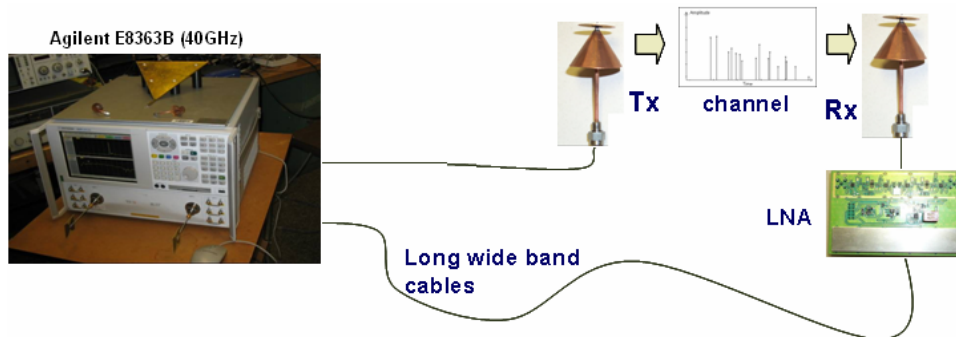
Figure 3: Measurement system used for UWB Ranging Errors.

The overall measurement system has a noise level of -120 dBm. The undesirable effects of the cables, LNA and antennas are removed through system calibration. System calibration involves connecting the cables back-to-back without the antennas. This will remove the delay and attenuation of the cables. The second step to system calibration is connecting the antennas and performing a 1-meter LOS free space calibration. This removes the delay and gain caused by the antennas. As a result the CIR after calibration in this case would be a single path occurring at 0 ns.

3.2 Measurement scenario

The measurements were conducted in the Atwater Kent (AK) building which houses the ECE department of the Worcester Polytechnic Institute (WPI), Worcester, MA. We have compiled a database of 670 UWB channel measurements with distances varying from 1 to 30m.

Measurements were conducted on the three floors of the building, shown in Fig. 4. The first floor focused on outdoor-indoor measurements where two different transmitter locations created the measurement sets. The second floor measurements focused on the effect of inter-office walls where four transmitter locations produced four different measurement scenarios. The third floor measurements took advantage of the existence of a metallic chamber. Three transmitter locations created three different measurement sets. The significance of this metallic chamber is to act as a harsh obstacle on the direct path between the transmitter and receiver causing a number of UDP measurements. The variety of measurements on the three floors of AK provides a rich and diversified database of scenarios that is significant for the modeling of both the path-loss and ranging errors.

3.3 Post processing of measurements

In the post-processing of channel measurement data, in order to obtain the time-domain CIR, the frequency domain measurements are passed through the inverse Fourier transform followed by Hanning window. The TOA and amplitude of multipath components are detected from time-domain channel profile with a peak detection algorithm. The noise threshold for peak detection is set to -115dB. The use of Hanning window produces a dynamic range of 32dB. Even though some other window functions such as the Kaiser window provides higher dynamic range, the Hanning window is selected for its much faster decaying side-lobes which significantly reduces the interfering effect of strong multipath components in peak detection. Samples of channel profile measurements for DDP and UDP conditions are shown in Fig. 5. With the channel measurement bandwidth of 1GHz, time-domain resolution of the measurement is about 0.71ns, which corresponds to 0.21m in distance. Therefore, if the detected τ_1 is within this resolution to the τ_{DP}, we may claim that the DP is detected. In our database, 51.8% measurements have the DP detected.
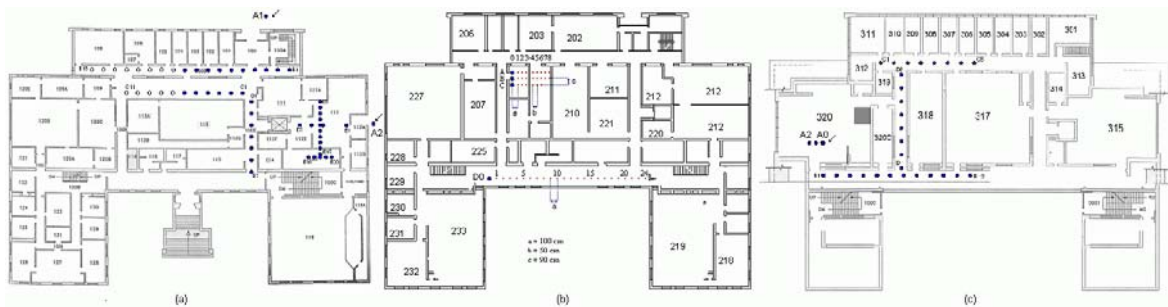
Figure 4: Floor plans of the measurements in Atwater Kent (AK), (a) First floor, (b) Second floor, (c) Third floor

5
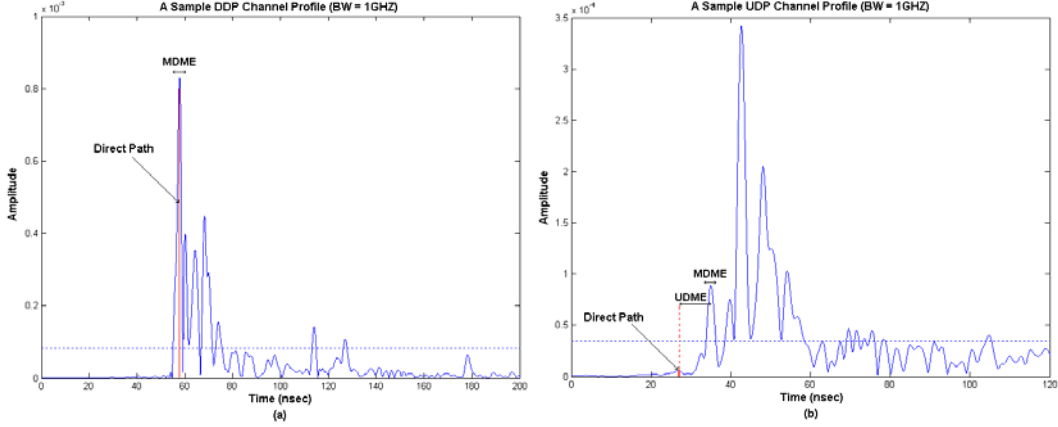
Figure 5: Ranging error in two different types of channel profiles (BW = 1 GHz), (a) UDP, (b) DDP.

4   Path-Loss Models for Ranging Systems

Using post processed UWB measurement described in section 3; in this section we present our empirical path-loss models. In the performance study of communication systems, path-loss model is normally developed for total received power. However as we explained earlier, in the study of ranging systems, path-loss models are needed for both DP and total received power. The path-loss model for DP determines the coverage for accurate ranging, and the path-loss model of total power determines system coverage in general. If the DP power is below signal detection threshold, ranging error occurs, while if the total received power is below the detection threshold, the ranging system loses its coverage.

Figure 6 shows the empirical partitioned path-loss models, developed from the UWB measurements described in section 3, for both DP and total power. The distance-power gradient is determined from measurement data using least-square (LS) linear regression [Pah05]. The partitioned model is defined as,

$$L_p = L_0 + \begin{cases} 10\alpha_1 \log_{10} d + \sigma_1, & d < d_{bp} \\ 10\alpha_1 \log_{10} d_{bp} + 10\alpha_2 \log_{10}(\dfrac{d}{d_{bp}}) + \sigma_2, & d \geq d_{bp} \end{cases} \tag{2}$$

where L_p is the path-loss in dB, L_0 is the first-meter path-loss, and d_{bp} is break-point distance.
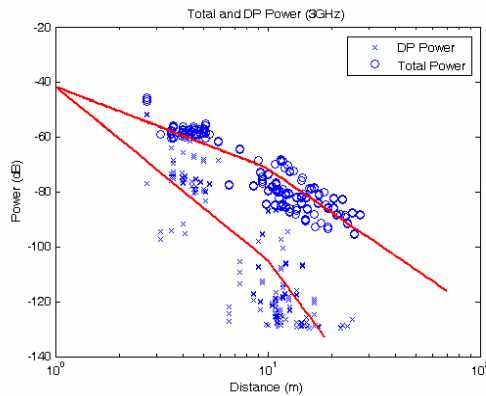
Figure 6: Partitioned path-loss models for direct-path and total power.

6

The path-loss is modeled with two different distance-power gradients α_1 and α_2, for before and after the break-point, respectively [Pah05]. The break-point designates the dividing point for LOS and NLOS channel conditions. In statistical channel modeling, the break-point distance is recommended to be 10m in indoor environment and the Fresnel zone for micro-cell environment [Pah05, Cas02]. Here our finding is consistent with previous results and we use 10m as for the break-point. Values for distance-power gradient α and the root-mean-square-error (RMSE) σ_x of linear regression for each model are shown in Table 1.

Table 1: Parameters of path-loss models derived from the UWM measurements.

	DP Power	Total Power
L_0 (dB)	-42	-42
d_{bp} (m)	10	10
α_1	6.0	3.0
α_1	10.2	5.3
σ_1 (dB)	14.5	5.0
σ_1 (dB)	12.1	5.5

In statistical channel modeling, a lognormal-distributed random variable is usually introduced to the deterministic models defined in (2) to model the shadow fading effects [Pah05]. The standard deviation (STD) of lognormal shadow fading can be determined as the RMSE of regression errors shown with σ1 and σ2 in (2) and in Table 1. In simulations one can also set this value to 10dB as widely used in the literature [Pah05]. Due to shadow fading in indoor environment, in reality the three regions, DDP, UDP and NC, defined earlier is not clearly divided as in Fig. 2. From the measurement results, we observed that when the distance is smaller than d_{bp}, ranging error is very small in general; but when distance is greater than d_{bp}, ranging error varies significantly with very large errors at some locations. Therefore, we can estimate the value of d_{UDP} with d_{bp}, and similarly we can estimate the value of d_{NC} with 30m. Considering shadow fading effect, we can roughly designate the region with distance of less than d_{bp} as DDP region, and from the break-point to 30m as a mixture of DDP and UDP and the region with greater than 30m as NC region.

The path-loss models developed in this section are important not only in the design and performance study of ranging and positioning techniques, but also in the design of system infrastructure deployment architectures. In the next section, we introduce an important benchmark for performance evaluation of positioning systems and analyze that based on the partitioning introduced in this section.

5   Analyzing the Accuracy of Ranging Systems

Performance of ranging systems can be measured by the amount of error that they exhibit in each ranging. As we discussed earlier, we refer to this error as DME and it is a function of bandwidth of the positioning system. To consider the effects of bandwidth we refer to ranging error as,

$$DME_W = \hat{d}_W - d \tag{3}$$

where subscript *W* represents the system bandwidth.

Figure 5 shows two types of channel profiles from UWB measurements in two different detection regions. Figure 5-(a) shows a DDP situation, while Fig. 5-(b) shows a case that the DP is not detected, i.e. a UDP case. In both cases we detect the first available peak, which is the peak above the threshold. The level of detection threshold is determined by the noise power and dynamic range of the receiver, and the side-lobe amplitude of the peaks that depends on the selected window.

In the first case, the first peak is mainly created by the DP. But because of the multipath effect it has deviated around the DP. If we assume that the physical measurement error is negligible, this deviation from the DP, shown with a two sided horizontal arrow on top of the peak, is the error caused by multipath components close to the DP. In [Ala03-a, b] it is shown that this type of error can be modeled as a zero-mean Gaussian random variable with a variance which depends on the distance. We refer to this error as multipath DME (MDME) and we show that its variance reduces by increasing the bandwidth.

On the other hand, in the second channel profile, the FDP does not contain the DP anymore. In fact the DP is been weakened so much that it is below the detection threshold. This situation introduces a new type of error that we call it UDP-DME (UDME). It is interesting to know that also in UDP situation since there are some paths close to the detected path the MDME component still exists but this time it adds to the UDME, which changes the position of the detected peak. Therefore the DME can be written as follows,

$$DME_W = \begin{cases} MDME_W & \text{DDP Region} \\ MDME_W + UDME_W & \text{UDP Region} \end{cases} \tag{4}$$

But because of the shadow fading most of the times we don't have information about the region. In this case we can rewrite (4) as a summation of a MDME, which always exists, and UDME that some times happens. We model the occurrence of the UDP condition with the random variable $\xi_W(d)$ that takes value of "1" when a UDP condition occurs and "0" otherwise. Therefore, our model for the DME is given by,

$$DME_W = MDME_W + \xi_w \cdot UDME_W \tag{5}$$

In the next section we use the empirical data to develop a statistical model for all components of (5) as a function of system bandwidths and the distance between the transmitter and the receiver.

6 Statistical Modeling of Distance Measurement Error

In the previous section it was shown that DME consists of two different components, MDME and UDME. Therefore in the next two subsections each of them will be modeled separately.

6.1 Modeling of MDME

To determine the model parameters from the empirical data we have partitioned our database of DMEs for each given bandwidth into DDP (detected DP) and UDP. The DDP distance measurement error database represents cases which are only disturbed by MDME and in this subsection we use only those for modeling.

Figure 7-a shows the scatter plot of MDME versus distance, d, for DDP channel profiles and bandwidth of 100 MHz. Naturally one expects an increase in the distance measurement error with the increase of distance between the transmitter and the receiver. Our observation from the empirical measurement results shows that this increase has a nonlinear relation. Therefore, to proceed with our modeling of MDME, we introduce parameter γ_W, the normalized ranging error,

$$\gamma_W = \frac{MDME(d)}{\log(1+d)}. \tag{6}$$

The logarithm in the denominator is used to accommodate the increase pace of error below linear. The scatter plots of γ_w are shown in Fig. 7-b. It can be seen that the normalization factor has compensated the distance effect. Our measurement results show that this normalization causes the resulting normalized error to form a Gaussian distribution. Therefore, the MDME has been modeled as,

$$MDME(d) = \gamma_W \, \log(1+d) \tag{7-a}$$

$$\gamma_W \sim N\left(m_{M,W}, \sigma_{M,W}\right) \tag{7-b}$$

Where, $N(m_{M,W}, \sigma_{M,W})$ is a Gaussian distribution with mean $m_{M,W}$ and variance $\sigma^2_{M,W}$. Table 2 displays typical values of these parameters.
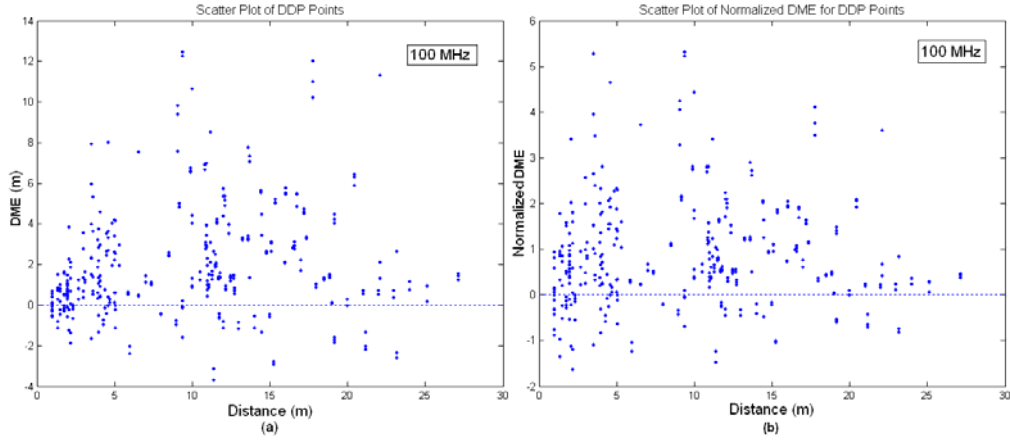
Figure 7: Scatter Plots of (a) $\varepsilon_{M,W}$, (b) γ_W versus distance for 100MHz Bandwidth.

Table 2: Typical values of model parameters derived from the measurements results.

W (MHz)	$m_{M,W}$ (m)	$\sigma_{M,W}$ (cm)	$P_{closeU,W}$	$P_{farU,W}$	$m_{U,W}$ (m)	$\sigma_{U,W}$ (cm)
20	3.66	515	0	0.005	−12.83	0
50	1.57	205	0	0.009	24.48	21.1
100	0.87	115	0	0.091	5.96	358.5
200	0.47	59	0.006	0.164	3.94	289.0
500	0.21	26.9	0.064	0.332	1.62	80.9
1000	0.09	13.6	0.064	0.620	0.96	60.4
2000	0.02	5.2	0.070	0.740	0.76	71.5
3000	0.004	4.5	0.117	0.774	0.88	152.2

6.2 Modeling of UDME

In order to model the UDP distance measurement errors we need to model two parameters, $\xi_W(d)$ and UDME. The random variable $\xi_W(d)$ is a binary random variable with the probability density function shown in (8-a), where $P_{U,W}(d)$ is the probability of occurrence of UDP for a given bandwidth.

The $P_{U,W}(d)$, however, is also a function of distance. Based on the results of path-loss modeling for total power and the DP presented in section 4 we assume that the probability of

UDP in locations close to the transmitter and locations far from the transmitter are substantially different and we need to partition the model. We use the 10m break-point found in section 4 to partition the behavior of the error in the two regions. Then for distances shorter than the break-point $P_{U,W}(d)$ is modeled as $P_{close\,U,W}$ and beyond the break point as $P_{far\,U,W}$.

$$f_{\xi_W}(y) = \left(1 - P_{U,W}(d)\right)\delta(y) + P_{U,W}(d)\delta(y-1) \tag{8-a}$$

$$P_{U,W}(d) = \begin{cases} P_{close\,U,W} & d \leq 10\,m \\ P_{far\,U,W} & d > 10\,m \end{cases} \tag{8-b}$$

Table 2 shows approximations to $P_{close\,U,W}$ and $P_{far\,U,W}$ for different bandwidths. As Rx moves away from Tx the DP power decreases, resulting in an increase in the probability of occurrence of the UDP condition.

To model UDME we estimate the distribution of UDME with non-zero mean Gaussian random variable. Figure 8 shows two PDFs for two different bandwidths, plotted against the model. Table 2 shows the values of m_w and $\sigma^2_{U,w}$ for different bandwidths obtained from the measurements.

$$UDME_W \sim N\left(m_{U,W}, \sigma_{U,W}\right) \tag{9}$$
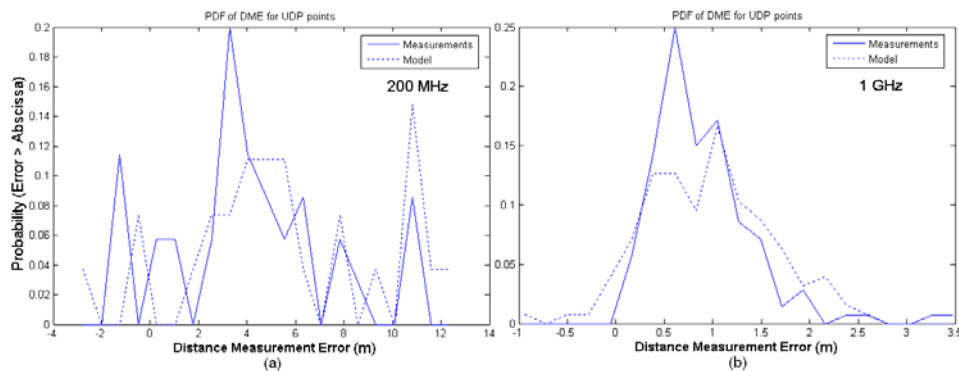
Figure 8: Comparison between the distribution of UDME for model and measurements for (a) 200 MHz, (b) 1GHz

6.3 The General Model for Distance Measurement Error

If we combine our results of multipath and UDP modeling, the overall model for estimated distance measurement is,

$$\hat{d} = d + MDME_W + \xi_W(d)UDME_W$$
$$= d + \gamma_W \log(1+d) + \xi_W(d)UDME_W \tag{10}$$

where,

$$f_{\xi_W}(y) = \left(1 - P_{U,W}(d)\right)\delta(y) + P_{U,W}(d)\delta(y-1) \tag{11}$$

This model relates the ranging error to the distance and bandwidth of the system. Figure 9 compares the complementary CDF of the ranging error obtained from empirical UWB measurements and the overall model described by (10) and (11) for bandwidths of 200MHz and 1GHz. The bandwidth of the UWB measurements taken at 3-6GHz is adjusted to these two values to provide a fair comparison. The model shows close agreement with the empirical data.
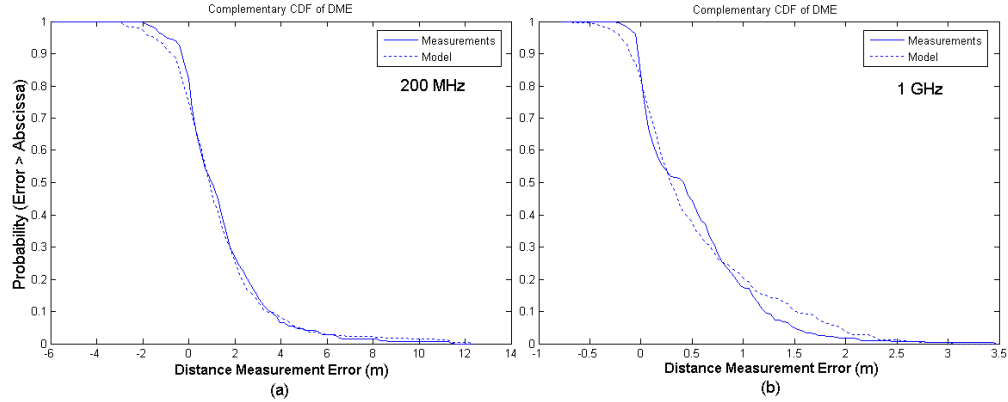
Figure 9: CDF comparisons between measurements and model for total points, (a) BW = 200 MHz, (b) BW = 1 GHz.

7   Conclusion

In this paper, using UWB measurements in an office building we developed indoor geolocation specific path loss models for both DP and total power. Based on these models we showed that the frequent occurrence of UDP conditions in NLOS areas is unavoidable. We also demonstrated that an increase in the distance can increase the chance of having UDP and increasing the system bandwidth decreases DME. Based on these observations, we introduced a novel model for the ranging error or DME in NLOS areas which separated the causes of the DME into multipath and UDP conditions and related them to the system bandwidth and the distance between the transmitter and the receiver. Finally, we demonstrated that the results of our model closely fit the empirical UWB data collected in an office building.

Acknowledgement

Authors would like to thank Dr. Allen H. Levesque for his valuable help in reviewing and editing this paper.

References

[Ala03a] B. Alavi and K. Pahlavan, "Bandwidth effect on distance error modeling for indoor geolocation," *Proc. IEEE 14th Annual IEEE International Symposium on Personal Indoor and Mobile Radio Communications (PIMRC 2003)*, Vol. 3, 7-10 Sept. 2003, pp. 2198 – 2202.

[Ala03b] B. Alavi and K. Pahlavan, "Modeling of The Distance Error for Indoor Geolocation", *Proc. IEEE Wireless Communications and Networking Conference (WCNC)*, 2003, Vol. 1, 16-20 March 2003, pp. 668 – 672.

[Ala05] B. Alavi and K. Pahlavan, "Analysis of Undetected Direct Path in Time of Arrival Based UWB Indoor Geolocation," *Proc. IEEE 62nd Vehicular Technology Conference 2005 (VTC-Fall 2005)*, 25-28 September 2005, Dallas, Texas.

[Cas02] D. Cassioli; M. Z. Win, A. F. Molisch, "The ultra-wide bandwidth indoor channel: from statistical model to simulations," *Selected Areas in Communications, IEEE Journal on* , Vol. 20, No. 6, Aug. 2002, pp. 1247 – 1257.

[Ghas03] S. S. Ghassemzadeh, L. J. Greenstein, A. Kaveiae, T. Sveinsson, and V. Tarokh, "UWB indoor delay profile model for residential and commercial buildings," *Proc. IEEE 58th Vehicular Technology Conference 2003 (VTC-Fall 2003)*, 6-9 October 2003, Lake Buena Vista, FL, Fall 2003, pp. 3120-3125.

[Ghav04] M. Ghavami, L. B. Michael, and R. Kohno, *Ultra-wideband Signals and Systems in Communication Engineering,* Wiley, Hoboken, NJ, 2004.

[Has93] H. Hashemi, "The indoor radio propagation channel," *Proc. IEEE,* Vol. 81, pp. 943-968, 1993.

[How90] S.J. Howard and K. Pahlavan, "Measurement and analysis of the indoor radio channel in the frequency domain," *Instrumentation and Measurement, IEEE Transactions on,* Vol. 39, No. 5, Oct. 1990, pp. 751 – 755.

[Li04] X. Li and K. Pahlavan, "Super-resolution TOA estimation with diversity for indoor geolocation," *IEEE Trans. on Wireless Communications,* Vol. 3, No. 1, Jan. 2004, pp. 224-234.

[Mol03] A.F. Molishch, J.R. Foerster, and Marcus Pendergrass, "Channel models for ultrawideband personal area networks," *IEEE Wireless Communications*, Vol. 10, No. 6, Dec. 2003, pp. 14 - 21.

[Opp04] I. Oppermann, M. Hamalainen, and J. Iinatti, *UWB Theory and Applications,* Wiley, Hoboken, NJ, 2004.

[Pah98] K. Pahlavan, P. Krishnamurthy, and J. Beneat, "Wideband Radio Channel Modeling for Indoor Geolocation Applications," *IEEE Communication Mag.,* Vol. 36., No. 4, Apr. 1998, pp. 60-65.

[Pah02] K. Pahlavan, X. Li, and J. P. Makela, "Indoor Geolocation Science and Technology," *IEEE Communication. Magazine.*, Vol. 40, No. 2, Feb. 2002, pp. 112-118.

[Pah05] K. Pahlavan, A. H. Levesque, *Wireless Information Networks*, Second Edition, Wiley-Interscience, 2005.

[Por03] D. Porcino and W. Hirt, "Ultra-wideband radio technology: potential and challenges ahead," *IEEE Communications Magazine*, Vol. 41, No. 7, July 2003, pp. 66 - 74.

[Rap02] T. S. Rappaport, *Wireless Communications:Principles and Practice*, 2nd ed., Prentice Hall, Upper Saddle River, NJ, 2002.

[Sal87] A. M. Saleh and R. A. Valenzuela, "A statistical model for indoor multipath propagation," *IEEE Journal on Selected Areas in Communication.* JSAC-5, pp 128-137, 1987.